

Article

Recycle Effect on Device Performance of Wire Mesh Packed Double-Pass Solar Air Heaters

Chii-Dong Ho *, Chun-Sheng Lin, Tz-Jin Yang and Chun-Chieh Chao

Department of Chemical and Materials Engineering, Tamkang University, 151 Yingzhuang Road, Tamsui District, New Taipei 251, Taiwan; E-Mails: cicadas0908@hotmail.com (C.-S.L.); kgftdog@hotmail.com (T.-J.Y.); tokyo363@gmail.com (C.-C.C.)

* Author to whom correspondence should be addressed; E-Mail: cdho@mail.tku.edu.tw; Tel.: +886-226-215-656 (ext. 2724); Fax: +886-226-209-887.

External Editor: Chi-Ming Lai

Received: 5 September 2014; in revised form: 30 October 2014 / Accepted: 4 November 2014 /

Published: 18 November 2014

Abstract: A new device for inserting an absorber plate to divide a flat-plate channel into two subchannels to conduct double-pass wire mesh packed operations was developed. The proposed wire mesh packed device improves the heat transfer efficiency substantially as compared that to flat-plate single-pass and double-pass operations using the same working dimensions, and the improvement of device performance was investigated experimentally and theoretically. Good agreement between the theoretical prediction and the measured values from the experimental results was achieved. Considerable heat transfer improvement was obtained employing wire mesh packed double-pass operations under the absorber plate with external recycle. The influences of recycle ratio on the heat transfer efficiency and the power consumption increase were also discussed.

Keywords: wire mesh; recycle; heat transfer efficiency; double-pass; solar air heater

1. Introduction

Low temperature energy technology solar collectors are a special kind of heat exchanger that transforms solar radiation energy into internal energy of the working fluids flowing through the heat exchanger devices. Solar radiation collection by solar collectors has attracted a great deal of interest in

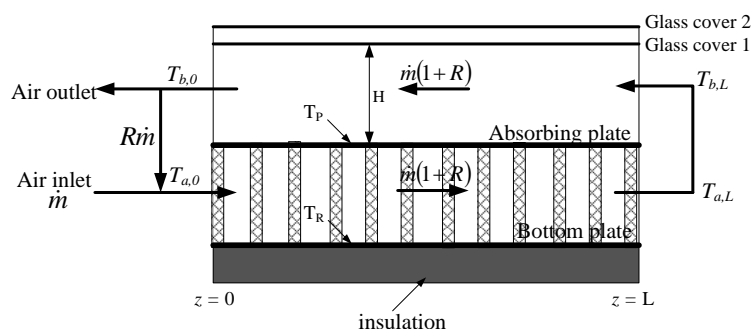
recent years, and these devices are widely used, mostly for heating both water and air fluids. Solar air collectors are less complicated and easy to implement coupled with existing space heating and drying systems [1], drying agricultural products [2,3] and some industrial applications [4,5]. The underside of the absorber plate and the edge of casing are well insulated to reduce conduction losses while the transparent covers on the top are used to reduce convection losses.

In addition to the effects of forced convection [6] and free convection [7,8], a considerable improvement on collector performance is achievable by increasing the heat-transfer area and creating air turbulence inside the flow ducts by using extended heat-transfer areas [9], air turbulence [10] and packing materials [11,12]. The higher convective heat-transfer coefficient and higher thermal energy efficiency are achieved in the solar collector of the present recycling device as the wire mesh is inserted in the lower channel under the absorber plate. Experimental and theoretical researches are undergoing simultaneously to design and modify the augmentation of double-pass solar air heaters [13–15]. Thanks to the packing wire mesh in the duct of solar air heaters for enhancing the thermal performance, the impacts of artificial turbulence were investigated in several papers [16–19], where the friction loss due to the packing wire mesh was studied as well. Thus, Kolb *et al.* [20] concluded that the presence of packing wire mesh in a flowing duct not only enhances both the convective heat transfer coefficient and the collector efficiency, but also increases the relatively small friction losses as compared to the conventional open channel [21]. Moreover, the forced convection enhancement due to the recycle-effect application in double-pass operations has been reported in numerous heat- and mass-transfer problems such as loop reactors [22], air-lift reactors [23], draft-tube bubble columns [24] and thermal diffusion columns [25], resulting in improved device performance. In the present work, a new double-pass solar air heater configuration that is actually the extension of the previous work [26], is studied theoretically and experimentally by adding packing wire mesh into the lower subchannel under recycling operation. An attempt has been made in the present study to: (a) provide a brief outline of both theoretical predictions and experimental results in the a wire mesh packed double-pass solar air heater; (b) discuss the exaggeration of the device performance of the effects of recycle ratio and wire mesh packing; and (c) examine the economic considerations regarding both heat-transfer efficiency improvement and power consumption increase.

2. Mathematical Modeling

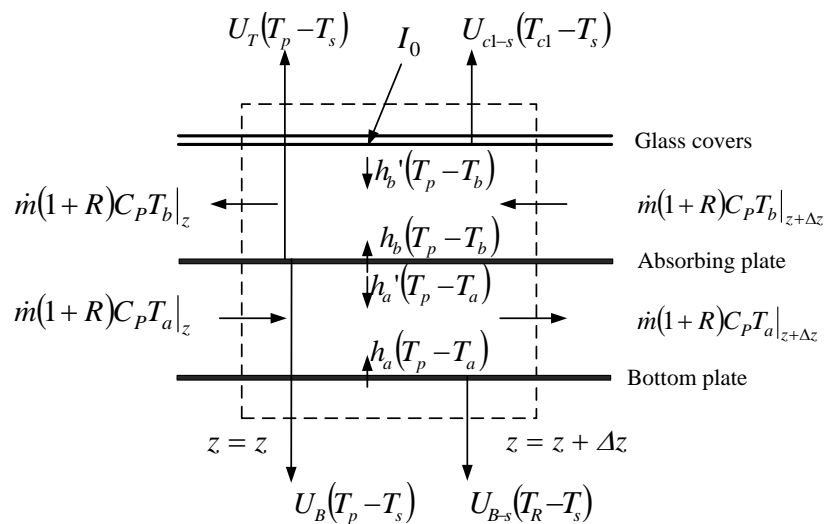
Consider a recycling double-pass solar air heater with inserting an absorber plate to divide a parallel conduit with height H , length L , and width W , as shown in Figure 1.

Figure 1. A schematic drawing of a wire mesh packed double-pass solar air heater.



The energy-flow diagram for a finite system element used for making an energy balance equation is presented in Figure 2. Before entering the lower subchannel in a double-pass device, the airflow (with air mass flow rate \dot{m} and inlet temperature T_{in}) will mix with the recycling airflow $R\dot{m}$ and $T_{b,0}$ exiting from the upper subchannel. A conventional blower situated at the beginning of the lower channel controls the recycling air mass flow rate. The following assumptions were made in this analysis: (1) the temperatures of the absorbing plate, bottom plate and bulk fluid are functions of the flow direction only; (2) both the glass covers and fluids do not absorb radiant energy; (3) the radiant energy absorbed by the glass cover 2 (outer cover) is assumed to be negligible; and (4) all outside surfaces of the solar air collector, except the glass cover, are well insulated thermally. With the above assumptions the energy equations may be written as indicated.

Figure 2. The energy balance on energy flow within a finite fluid element.



2.1. Temperature Distributions on Wire Mesh Packed Solar Air Heaters

The temperature distributions of both upper and lower subchannels can be obtained by solving the energy balance equations for the absorber plate, glass cover, airflow and bottom plate. By following the similar mathematical treatment performed in our previous work [26], two simultaneous ordinary differential equation were obtained providing energy balances for the glass cover, absorber plate, bottom plate and both upper and lower subchannels, and rearranging with some algebraic equation manipulations as follows:

$$\frac{d(T_b(\xi) - T_s)}{d\xi} = B_1 [T_b(\xi) - T_s] + B_2 [T_a(\xi) - T_s] + B_3 \tag{1}$$

$$\frac{d(T_a(\xi) - T_s)}{d\xi} = B_4 [T_b(\xi) - T_s] + B_5 [T_a(\xi) - T_s] + B_6 \tag{2}$$

and thus, we get the analytical solutions of the temperature distributions of the flowing air in both lower and upper subchannels:

$$T_a(\xi) = k_1 e^{y_1 \xi} + k_2 e^{y_2 \xi} + \frac{B_3 B_4 - B_1 B_6}{B_1 B_5 - B_2 B_4} \tag{3}$$

$$T_b(\xi) = \frac{Y_1 - B_5}{B_4} k_1 e^{Y_1 \xi} + \frac{Y_2 - B_5}{B_4} k_2 e^{Y_2 \xi} + \frac{B_2 B_6 - B_3 B_5}{B_1 B_5 - B_2 B_4} \tag{4}$$

The definitions of B_i and Y_i are described in the Appendix, and the constants k_1 and k_2 in Equations (3) and (4) were determined with the use of the following boundary conditions:

$$\xi = 0, T_a(0) = T_{a,0} = \frac{T_{in} + RT_b(0)}{1 + R} \tag{5}$$

$$\xi = 1, T_a(1) = T_{a,L}, T_b(1) = T_{b,L}, \text{ and } T_{b,L} = T_{a,L} \tag{6}$$

2.2. Heat Transfer Coefficients of Wire Mesh Packing

The equivalent hydraulic diameter $D_{e,a}$ and $D_{e,b}$ of both subchannels in double-pass devices and $D_{e,0}$ in the single-pass one, respectively, can be expressed by the characteristic length in the present devices:

$$D_{e,a} = 4r_h = \frac{Pd_w}{1 - P}, D_{e,b} = \frac{4WH}{(W + H)}, D_{e,0} = \frac{4W(2H)}{(W + 2H)} \tag{7}$$

which the hydraulic radius r_h for the lower subchannel of wire mesh packing conduit was defined by Varshney and Saini [27], and the porosity P of the wire screen matrix was defined by Chang [28]:

$$P = 1 - \left(\frac{n\pi d_w^2}{2P_t D} \right) \left(1 + \frac{d_w^2}{P_t^2} \right)^{1/2} \tag{8}$$

The correlated equations for the upper subchannel were derived from Kays [29] and Heaton *et al.* [30] for turbulent flow and laminar flow, respectively, as follows:

$$Nu_b = 0.0158 Re_b^{0.8} [1 + (D_{e,b} / L)^{0.7}], \text{ for turbulent flow} \tag{9}$$

$$Nu_b = 4.4 + \frac{0.00398(0.7 Re_b D_{e,b} / L)^{1.66}}{1 + 0.0114(0.7 Re_b D_{e,b} / L)^{1.12}}, \text{ for laminar flow} \tag{10}$$

and the estimation equation for the wire mesh conduit was developed by Saini and Saini [31]:

$$Nu_a = \frac{h_a D_{e,a}}{k} = 4.0 \times 10^{-4} (Re_a)^{1.22} \left(\frac{P_t}{D_{e,a}} \right)^{0.625} \left(\frac{s}{10P_t} \right)^{2.22} \left(\frac{l}{10P_t} \right)^{2.66} \times \exp[-1.25(\ln \frac{s}{10P_t})^2] \exp[-0.824(\ln \frac{l}{10P_t})^2], Re_a > 1800 \tag{11}$$

2.3. Heat Transfer Coefficients and Collector Efficiency Improvement

The total heat loss coefficient was estimated from the solar air collector to the surroundings is the summation of top, edge and bottom loss rate, *i.e.*,

$$U_L = \left\{ U_T A_c (T_{p,m} - T_s) + U_B A_c (T_{R,m} - T_s) + U_E A_E [(T_{a,m} - T_s) + (T_{b,m} - T_s)] \right\} / A_c (T_{p,m} - T_s) \tag{12}$$

An empirical equation of U_T was developed [32] following the basic procedure [33] for the horizontal collector with two glass covers, as shown in Figure 1, in which the edge U_E and bottom U_B loss

coefficients depend mostly on the insulation thickness by conduction. Moreover, the thermal resistance from the inner glass cover to the ambient air may be calculated with the aid of the heat-transfer coefficient for free convection of air between two glass covers by using Hottel's empirical equation [33]. The convective heat-transfer coefficient for air flowing over the surface of outer glass cover was calculated using the following empirical equation given by McAdams [34]:

$$h_w = 2.8 + 3.0 V \quad (13)$$

The outlet temperature of $T_{b,0}$ can be calculated from Equation (7) with $\xi = 0$:

$$T_b(0) = T_{b,0} = \frac{Y_1 - B_5}{B_4} k_1 + \frac{Y_2 - B_5}{B_4} k_2 + \frac{B_2 B_6 - B_3 B_5}{B_1 B_5 - B_2 B_4} \quad (14)$$

The useful energy gained by the flowing air was calculated from the following relation once the inlet and outlet temperatures are determined:

$$Q_u = M_a A_c (T_{a,L} - T_{a,0}^0) + M_b A_c (T_{b,0} - T_{b,L}) = \dot{m} C_p (T_{b,0} - T_{in}) \quad (15)$$

The collector efficiency η_w of a wire mesh packed solar air heater that relates the actual useful energy gain from the incident solar radiation was defined by plugging Equation (12) into Equation (16) as follows:

$$\eta_w = Q_u / A_c I_0 = \tau_g^2 \alpha_p - U_L (T_{p,m} - T_s) / I_0 = \dot{m} C_p (T_{b,0} - T_{in}) / A_c I_0 = [-M_b / I_0 (1 + R)] (T_{b,0} - T_{in}) \quad (16)$$

Therefore, the average temperatures of the absorbing plate are readily obtained by rearranging Equation (16) as follows:

$$T_{p,m} = T_s + \left[I_0 \alpha_p \tau_g^2 - \frac{M_b}{1 + R} (T_{b,0} - T_{in}) / U_L \right] \quad (17)$$

The collector efficiency improvements, I_F and I_w , employing both flat-plate and wire mesh packed solar air heaters, respectively, are defined by the percentage increase in the collector efficiency related to a single-pass device under the same operating conditions as follows:

$$I_F = \frac{\eta_F - \eta_s}{\eta_s} \times 100\% \quad (18)$$

$$I_w = \frac{\eta_w - \eta_s}{\eta_s} \times 100\% \quad (19)$$

in which η_F , η_w and η_s , respectively, denote the collector efficiency in flat-plate type and wire mesh packed double-pass and downward-type single-pass solar air heaters.

The following are the system properties, operating conditions and essential physical properties employed in this study, as represented in Table 1. The method for theoretical prediction of collector efficiencies in the present study is similar to that developed in our previous work [26], except for the alternative configuration of the flow pattern. An initial value of η_w is calculated from Equation (16) coupled with the use of all appropriate equations for the given collector geometries, physical properties and operating conditions, once the average temperatures $T_{a,m}$, $T_{b,m}$ and $T_{p,m}$ are specified. The new guessed average temperatures $T_{a,m}$, $T_{b,m}$ and $T_{p,m}$ are then re-calculated using Equations (3), (4) and (17), respectively, with the iteration calculations until tolerance is small enough (say less than 1×10^{-3}).

After the accurate outlet air temperature of Equation (14) is obtained, the corresponding value of the collector efficiency η_w is thus obtained in Equation (16).

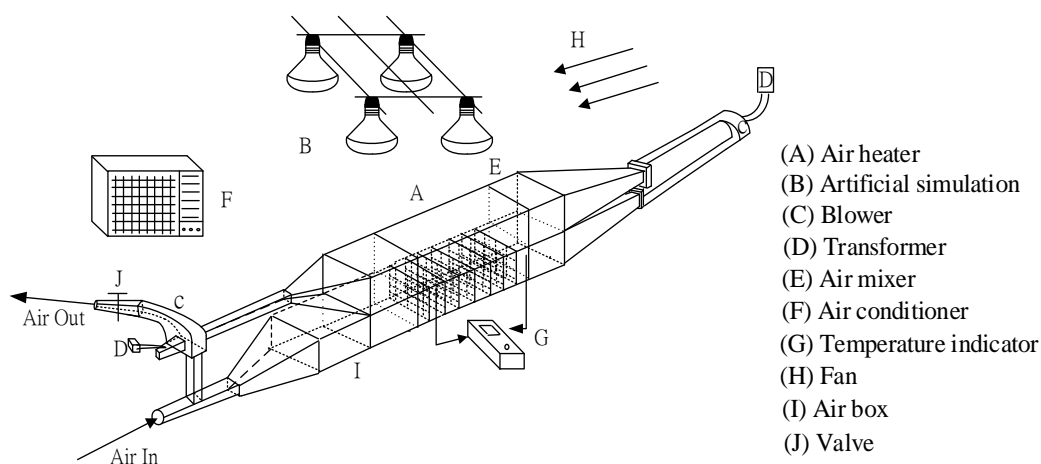
Table 1. Specifications of system properties, operating conditions and essential physical properties.

Parameters		Operation parameters		Physical properties	
A_c (m ²)	0.09	\dot{m} (kg/s)	0.0107, 0.0161, 0.0214	α_p	0.96
H (m)	0.05	T_{in} (°C)	20, 30, 40	ϵ_σ	0.94
L (m)	0.3	T_s (°C)	20 ± 0.1	ϵ_p	0.8
W (m)	0.3	I_0 (W/m ²)	830 ± 20, 1100 ± 20	ϵ_R	0.94
l (m)	0.015	V (m/s)	1.0	τ_σ	0.875
–	–	–	–	k_s (W/m K)	0.033

3. Experimental Procedure

A 0.3 m long and 0.3 m wide wire mesh packed double-pass solar air heater with external recycle was constructed of stainless steel and insulated using Styrofoam. Each flow channel was 0.05 m in height and the distance between the two glasses was 0.05 m. The collector consists of two glass covers, a black absorber plate, 20 pieces of mesh wire were welded underneath the absorber plate and perpendicular to air flowing direction with mesh interval of 0.015 m. A schematic diagram of an artificial simulation of a solar air heater is shown in Figure 3.

Figure 3. Experimental setup of a wire mesh packed double-pass solar air heater.



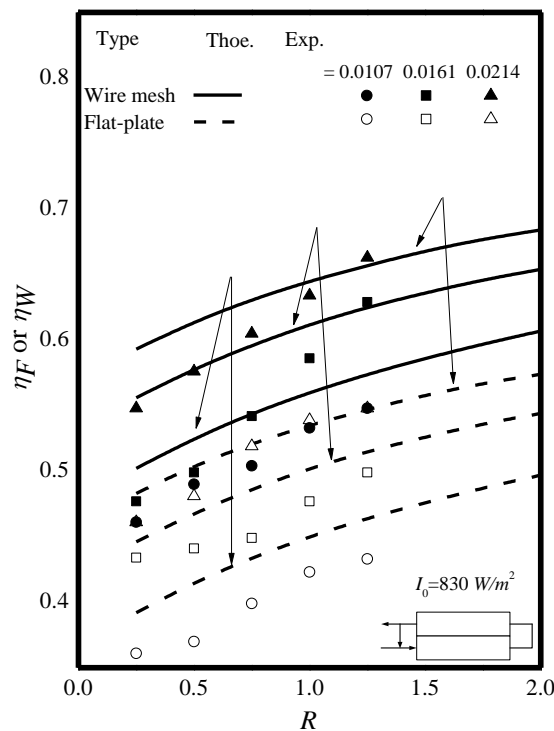
The ambient temperature ($T_s = (30 \pm 0.1)$ °C) was controlled by using an air conditioner and measured at a position 0.15 m above the outer glass cover. A fan provided an ambient steady airflow wind of 1.0 m/s (EUPA TSK-F1426, 14" EUPA, Xiamen, Fujian, China) in the experimental runs. The air temperatures at the inlet and outlet of the solar collector and the temperature of the absorber plate were measured with thermocouples (TFC-305A, Hwa Tai Technology Co, Ltd., Taipei, Taiwan). The ambient air was steadily supplied by a blower (Teco 3 Phase Induction Motor, Model BL model 552, Redmond Co., Owosso, MI, USA) and the flow rate was controlled by a transformer, while the flow rate was measured by an anemometer (Model 24-611, Kanomax Japan Inc., Osaka, Japan). Before entering the lower subchannel, the airflow with mass flow rate \dot{m} and temperature T_{in} will pre-mix the air flow

exiting from the upper subchannel with Rm and $T_{b,0}$ which is regulated by means of a valve situated at the end of the lower subchannel. One set of adjustable radiation sources consisted of 14 electrical energy supplies (110 V, 125 W) and was employed by using a set of on/off switches. The simulating incident solar radiation I_0 were measured and recorded with a Model No. 455 pyranometer (TSI Inc., St. Paul, Shoreview, MN, USA).

4. Results and Discussion

Both qualitative and quantitative agreements are achieved between theoretical and experimental results, as indicated in Figure 4 and Table 2 for flat-plate and wire mesh packed solar air heaters with incident solar radiation, air mass flow rate and recycle ratio as parameters.

Figure 4. Effect of the recycle ratio on collector efficiency in flat-plate and wire mesh packed solar air heaters with recycle.



The collector efficiency improvement increases with increasing recycle ratio and air mass flow rate in a more remarkable extent due to the convective heat-transfer coefficient enhancement by enlarging the fluid velocity. The accuracy of the theoretical predictions by measuring the deviation from the experimental results was estimated using the following definition as:

$$E = \frac{1}{N_{\text{exp}}} \sum_{i=1}^{N_{\text{exp}}} \left| \frac{\eta_{\text{theo},i} - \eta_{\text{exp},i}}{\eta_{\text{theo},i}} \right| \times 100\% \tag{20}$$

where N_{exp} , $\eta_{\text{theo},i}$ and $\eta_{\text{exp},i}$ are the number of experimental runs, theoretical prediction and experimental results of collector efficiencies, respectively.

Table 2. Theoretical predictions of heat transfer efficiency of η_F and η_w .

\dot{m} (kg/s)	R	$I_0 = 830 \text{ (W/m}^2\text{)}$		$I_0 = 1100 \text{ (W/m}^2\text{)}$	
		Flat-plate	Wire mesh	Flat-plate	Wire mesh
		η_F	η_w	η_F	η_w
0.0107	0.5	0.415	0.525	0.417	0.527
	1	0.450	0.560	0.452	0.562
	1.5	0.476	0.586	0.478	0.588
	2	0.497	0.607	0.498	0.608
0.0161	0.5	0.468	0.578	0.470	0.580
	1	0.502	0.612	0.503	0.613
	1.5	0.526	0.636	0.527	0.637
	2	0.544	0.654	0.545	0.655
0.0214	0.5	0.504	0.614	0.506	0.616
	1	0.535	0.645	0.537	0.647
	1.5	0.558	0.668	0.558	0.668
	2	0.574	0.684	0.575	0.685

The accuracy deviations are showed in Table 3 with two incident solar radiation I_0 for both configurations with and without attaching wire mesh, respectively.

Table 3. The deviation of the experimental results from theoretical predictions both in flat-plate type and wire mesh packed.

Accuracy	$E = \frac{1}{N_{\text{exp}}} \sum_{i=1}^{N_{\text{exp}}} \frac{ \eta_{\text{theo},i} - \eta_{\text{exp},i} }{\eta_{\text{theo},i}} \times 100\%$			
	Flat-plate		Wire mesh	
	\dot{m} (kg/s)	I_0 (W/m ²)	I_0 (W/m ²)	I_0 (W/m ²)
	830	1100	830	1100
0.0107	1.58	5.38	4.27	0.85
0.0161	5.09	5.92	9.44	5.15
0.0214	2.50	3.56	6.64	5.75

The agreement between the experimental results and theoretical predictions is fairly good with the error analysis of $1.58 \times 10^{-2} \leq E \leq 5.92 \times 10^{-2}$ and $8.50 \times 10^{-3} \leq E \leq 9.44 \times 10^{-2}$ for flat-plate and wire mesh packed devices, respectively, as shown in Table 3.

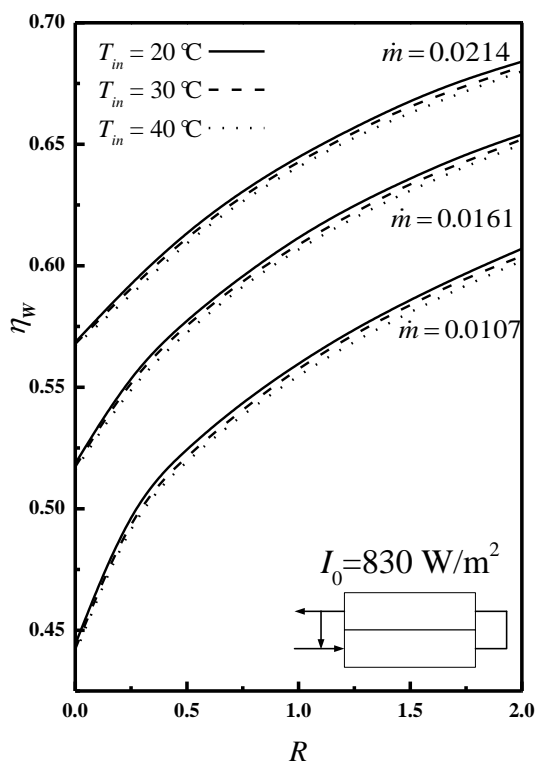
The theoretical and experimental results indicate that both collector efficiencies, η_F and η_w , increase with increasing recycle ratio and mass flow rate owing to the fluid velocity enlargement with enhancing the convective heat-transfer coefficient. Moreover, the theoretical predictions of I_F and I_w for the flat-plate and wire mesh packed double-pass devices, respectively, under various incident solar radiation, air mass flow rate and recycle ratio are presented in Table 4. The collector efficiency improvement, as shown in Table 4, is helpful in examining how collector efficiency improves with various operating parameters and design types. With this comparison, the advantage of the present device for all air mass flow rates, especially with $\dot{m} = 0.0107 \text{ kg/s}$ and $R = 2$ are 96.32% and 94.32%, respectively, for $I_0 = 830$ and $I_0 = 1100 \text{ W/m}^2$.

Table 4. Theoretical predictions of heat-transfer efficiency improvement of I_F and I_W .

m (kg/s)	R	$I_0 = 830 \text{ (W/m}^2\text{)}$		$I_0 = 1100 \text{ (W/m}^2\text{)}$	
		Flat-plate	Wire mesh	Flat-plate	Wire mesh
		I_F (%)	I_W (%)	I_F (%)	I_W (%)
0.0107	0.5	34.19	69.79	35.44	70.60
	1	45.62	81.22	46.77	77.29
	1.5	54.11	89.71	55.15	86.96
	2	60.72	96.32	61.68	94.32
0.0161	0.5	26.56	56.29	27.44	57.25
	1	35.58	65.31	36.36	66.17
	1.5	42.11	71.84	42.80	72.61
	2	47.10	76.83	47.73	77.54
0.0214	0.5	21.79	48.36	23.97	50.94
	1	29.33	55.90	31.51	58.47
	1.5	34.69	61.26	36.86	63.83
	2	38.73	65.30	40.91	67.87

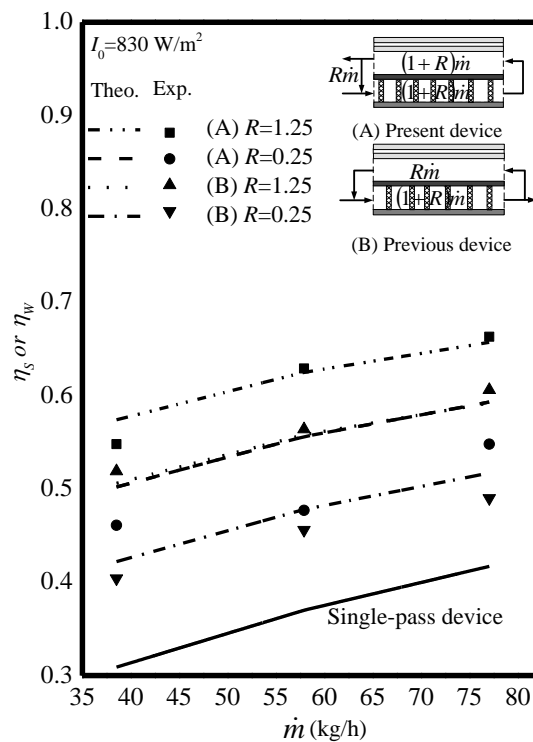
The influence of the inlet air temperature on the collector efficiency improvement is shown in Figure 5. The collector efficiency improvement increases with decreasing inlet air temperature. A double-pass solar air collector without recycle means $R = 0$ in the schematic drawing of a wire mesh packed double-pass solar air heater of Figure 1, and the theoretical predictions were also represented in Figure 5 for various inlet air temperatures. A device performance improvement is achieved in the present study as compared to a double-pass solar air collector without recycle, as indicated in Figure 5.

Figure 5. Effect of the inlet air temperature on collector efficiency in wire mesh packed solar air heaters with recycle ($I_0 = 830 \text{ W/m}^2$).



The present work is actually the extension previous work [26] except the recycle configuration. Figure 6 illustrates some theoretical predictions and experimental results obtained from [26] with the same design and operating parameters used in Figure 4 for comparison of the collector efficiency improvement. Further, both collector efficiencies, η_F and η_W , obtained in both devices increase with the air mass flow rate \dot{m} as a parameter, however, the increment in the present device was rather sensitive. This is because the larger amount of air flow, say $\dot{m}(1 + R)$, in the present device was heated in the upper subchannel and the extent of the higher improvement in the collector efficiency was achieved due to the desirable effect of the forced convection coefficient enhancement.

Figure 6. Comparisons of collector efficiency between the present and previous work [26].
Copyright 2013 Elsevier.



The power consumptions for the flat-plate, wire mesh packed and single-pass solar air heaters, respectively, may be estimated using empirical correlations as follows:

$$H_S = \dot{m} \ell w_{f,s} = \frac{2 f_{F,S} \bar{v}^2 L}{D_{e,S}} \tag{21}$$

$$H_{D,i} = \dot{m}(1+R) \ell w_{f,a} + \dot{m}(1+R) \ell w_{f,b} = \dot{m}(1+R) \frac{2 f_{F,a} \bar{v}^2 L}{D_{e,a}} + \dot{m}(1+R) \frac{2 f_{F,b} \bar{v}^2 L}{D_{e,b}}, \quad i = F, W \tag{22}$$

in which:

$$f_{F,a} = 3.5722 \times (1/nP)^{1.0431} (P_t/d_w)^{1.1507} Re_a^{-0.43}, \quad \text{for } Re_a > 1900, \text{ for wire mesh device [35]} \tag{23}$$

$$f_{F,i} = \frac{24}{Re}, \quad \text{for } Re < 2100, \quad i = a, b, S, \text{ for flat-plate device [36]} \tag{24}$$

$$f_{F,i} = \frac{0.0791}{Re^{0.25}}, \text{ for } 2100 < Re < 100,000, i = a, b, S, \text{ for flat-plate device [36]} \tag{25}$$

The calculated results of hydraulic dissipated energy in a single-pass device are $H_s = 1.8 \times 10^{-4}$, 5.72×10^{-4} and 1.25×10^{-3} , W for $\dot{m} = 0.0107$, 0.0161 and 0.0214 kg/s, respectively. The power consumption increments for flat-plate and wire mesh packed devices, $I_{P,W}$ and $I_{P,F}$, respectively, are defined as compared to that in the downward single-pass operation:

$$I_{P,W} = \frac{H_{D,W} - H_s}{H_s} \text{ for solar air heaters with wire mesh packed} \tag{26}$$

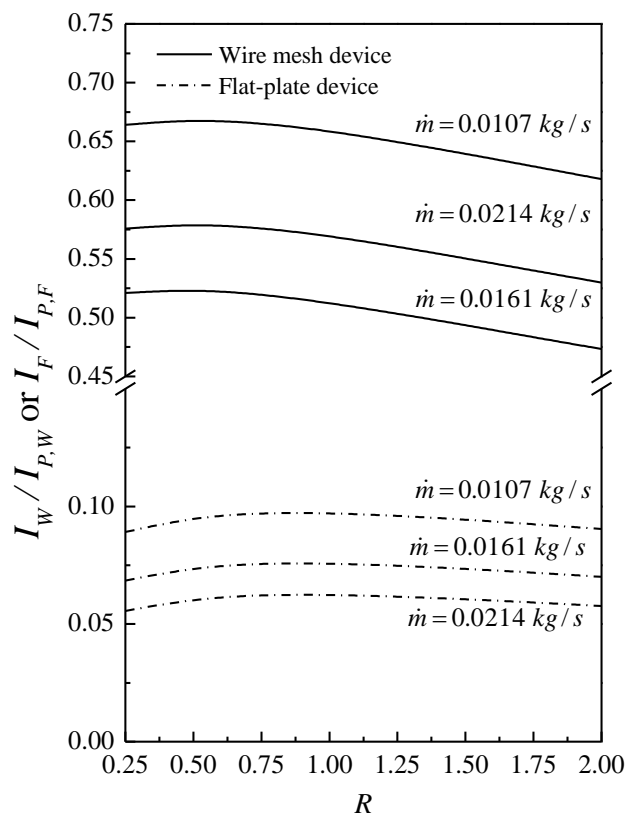
$$I_{P,F} = \frac{H_{D,F} - H_s}{H_s} \text{ for flat-plate double-pass solar air heater} \tag{27}$$

The hydraulic dissipated power consumption energy in operating both flat-plate type and wire mesh packed double-pass solar air heaters with external recycle are investigated with mass flow rate and recycle ratio as parameters, as shown in Table 5. The theoretical results show that the hydraulic dissipated energy increases with increasing mass flow rate and recycle ratio. An economic consideration of device performance is examined by evaluating both collector efficiency improvement and power consumption increment, $I_w/I_{P,W}$ and $I_f/I_{P,F}$, respectively, as illustrated in Figure 7. The effects of various recycle ratio and mass flow rate on $I_w/I_{P,W}$ and $I_f/I_{P,F}$ are presented graphically in Figure 7 for both flat-plate and wire mesh packed double-pass solar air heaters. These results reveal that an optimum operating condition exists between 0.5 and 1.0 for both flat-plate and wire mesh packed solar air heaters with various air mass flow rates and recycle ratios. Actually, there exists an economic selection in operating double-pass wire mesh packed solar air heaters at the optimal recycle ratio for the maximum value of $I_w/I_{P,W}$, which considers both the energy gain and energy consumption for making a good economic sense to achieve device operation profitability. Restated, the results confirm that the application of packing wire mesh to design a double-pass solar air heater is technically and economically feasible.

Table 5. The power consumption with recycle ratio and air mass flow rate as parameters.

R	Wire Mesh Packed ($H_{D,W}$)			Flat-Plate Type ($H_{D,F}$)		
	\dot{m} (kg/s)			\dot{m} (kg/s)		
	0.0107	0.0161	0.0214	0.0107	0.0161	0.0214
0.25	1.76×10^{-2}	5.05×10^{-2}	1.05×10^{-1}	7.44×10^{-4}	2.29×10^{-3}	5.01×10^{-3}
0.50	1.96×10^{-2}	5.61×10^{-2}	1.17×10^{-1}	8.53×10^{-4}	2.62×10^{-3}	5.74×10^{-3}
0.75	2.14×10^{-2}	6.13×10^{-2}	1.28×10^{-1}	9.58×10^{-4}	2.95×10^{-3}	6.44×10^{-3}
1.00	2.31×10^{-2}	6.62×10^{-2}	1.38×10^{-1}	1.06×10^{-3}	3.26×10^{-3}	7.12×10^{-3}
1.25	2.47×10^{-2}	7.08×10^{-2}	1.47×10^{-1}	1.16×10^{-3}	3.56×10^{-3}	7.78×10^{-3}
1.50	2.63×10^{-2}	7.52×10^{-2}	1.57×10^{-1}	1.25×10^{-3}	3.85×10^{-3}	8.42×10^{-3}
1.75	2.78×10^{-2}	7.95×10^{-2}	1.65×10^{-1}	1.34×10^{-3}	4.13×10^{-3}	9.04×10^{-3}
2.00	2.92×10^{-2}	8.35×10^{-2}	1.74×10^{-1}	1.43×10^{-3}	4.41×10^{-3}	9.65×10^{-3}

Figure 7. The values of $I_W/I_{P,W}$ and $I_F/I_{P,F}$ vs. recycle ratio with air mass flow rate as a parameter.



5. Conclusions

This study provides an alternative design for wire mesh packed solar air heaters with recycling operations. Significant improvements on the heat transfer efficiency are achieved by application of the recycle-effect concept to solar air heaters to conduct recycling double-pass operations. Recently, numerous papers have proposed exergy and energy analyses [37,38] to understand the effect of embedding a porous medium inside solar air heaters. The energy efficiency obtained in the case of an air mass flow rate of 0.02 kg/s is 0.5 in Figure 3 of [38], while at the air mass flow rate of 0.0214 kg/s and $T_{in} = 30$ °C in the present study, the value of collector efficiency is 0.52 with $R = 0$ in Figure 5. The agreement of both results achieved by embedding a porous medium and inserting a wire mesh, respectively, is pretty good. The device performance of wire mesh double-pass solar air heaters with external recycle was investigated theoretically and experimentally with the aim of making economic sense with consideration of the hydraulic dissipated energy. Meanwhile, theoretical predictions of the collector efficiency as well as the ratio of efficiency improvement and power consumption increment, say $I_W/I_{P,W}$, in recycling wire mesh double-pass solar air heaters were carried out and calculated with air mass flow rate and recycle ratio as parameters. The results show that the wire mesh packed solar air heater is economically feasible to improve the collector efficiency under recycling operation due to the promotion of turbulence intensity. This work indicates that a suitable selection of operating conditions for the new design of recycling wire mesh packed solar air heater could enhance collector efficiency with a reasonable hydraulic dissipated energy increase.

Acknowledgments

The authors wish to thank the Ministry of Science and Technology of the Republic of China for its financial support.

Author Contributions

This paper is a result of the full collaboration of all the authors. However, the concept for this research was conceived by Chii-Dong Ho, Chun-Sheng Lin contributed to mathematical derivations, Tz-Jin Yang elaborated the manuscript preparation and Chun-Chieh Chao performed the experiments.

Nomenclature

A_c	surface area of the collector = LW (m^2)
A_E	surface area of the edge of collector (m^2)
B_i	coefficients defined in Equations (A1)–(A6)
C_P	specific heat of air at constant pressure ($J/(kg \text{ K})$)
d_w	wire diameter of screen (m)
D	depth of the bed
$D_{e,0}$	equivalent diameter of downward-type single-pass device (m)
$D_{e,a}$	equivalent diameter of lower subchannel of double-pass device (m)
$D_{e,b}$	equivalent diameter of upper subchannel of double-pass device (m)
$D_{e,S}$	equivalent diameter of downward-type single-pass device
E	deviation of the experimental measurements from theoretical predictions, defined in Equation (20)
$f_{F,i}$	Fanning friction factor
F_i	coefficients defined in Equations (A20)–(A22)
G_i	coefficients defined in Equations (A9)–(A15)
H	height of both upper and lower subchannels (m)
$H_{D,i}$	The power consumptions for the flat-plate and wire mesh packed, defined in Equations (22) (W)
h_a	convection coefficient between the bottom and lower ($W/(m^2 \text{ K})$)
h_b	convection coefficient between the absorber plate and upper ($W/(m^2 \text{ K})$)
h_{c1-c2}	convection coefficient between the inner glass cover and outer glass cover ($W/(m^2 \text{ K})$)
$h_{r,c1-c2}$	radiation heat transfer coefficient between two covers ($W/(m^2 \text{ K})$)
$h_{r,c1-s}$	radiation heat transfer coefficient from cover 2 to the ambient ($W/(m^2 \text{ K})$)
h_{r1}	radiation heat transfer coefficient between inner glass cover and absorber plate ($W/(m^2 \text{ K})$)
h_{r2}	radiation heat transfer coefficient between absorber plate and bottom plate ($W/(m^2 \text{ K})$)
h_w	convective heat-transfer coefficient for air flowing over the outside surface of glass cover ($W/(m^2 \text{ K})$)

I_i	coefficients defined in Equations (A23) and (A24)
I_F	percentage of collector efficiency improvement in flat-plate air heater, defined in Equation (18)
$I_{P,i}$	percentage of power consumption increment, defined in Equations (26) and (27)
I_W	percentage of collector efficiency improvement in wire mesh air heater, defined in Equation (19)
k	thermal conductivity of the stainless steel plate (W/(m K))
k_i	coefficients defined in Equations (A18) and (A19)
k_s	thermal conductivity of insulator (W/(m K))
L	channel length (m)
l	the maximum length of the mesh (m)
l_s	thickness of insulator (m)
$\ell_{w_{f,a}}$	lower subchannel friction loss of double-pass device (J/kg)
$\ell_{w_{f,b}}$	upper subchannel friction loss of double-pass device (J/kg)
$\ell_{w_{f,s}}$	friction loss of downward-type single-pass device (J/kg)
M_a	parameter defined in Equation (A8) (J/(s m ² K))
M_b	parameter defined in Equation (A7) (J/(s m ² K))
\dot{m}	total air mass flow rate (kg/s)
N_{exp}	the number of the experimental measurements
$N_{u,i}$	Nusselt number
n	number of screens in a matrix
P	porosity of mesh
P_t	pitch of wire mesh (m)
Q_u	useful energy gained by air (W)
r_h	hydraulic radius (m)
R	recycle ratio, reverse air mass flow rate divided by input air mass flow rate
Re_o	Reynolds number, $2\dot{m}R / \mu(W + 2H)$
Re_a	Reynolds number, $Pd_w \dot{m}(1 + R) / (1 - P)A_c \mu$
Re_b	Reynolds number, $2\dot{m}(1 + R) / \mu(W + H)$
s	shortway of mesh (m)
$T_a(\xi)$	axial fluid temperature distribution in the lower subchannel (K)
$T_b(\xi)$	axial fluid temperature distribution in the upper subchannel (K)
$T_{a,0}^0$	the mixing temperature of the subchannel a at $x = 0$ (K)
$T_{a,L}$	the temperature of the lower subchannel at $x = L$ (K)
$T_{a,m}$	the mean temperature of the lower subchannel (K)
$T_{b,0}$	the temperature of the upper subchannel b at $x = 0$ (K)
$T_{b,L}$	the temperature of the upper subchannel b at $x = L$ (K)
$T_{b,m}$	the mean temperature of the upper subchannel (K)
$T_{b,o}$	the temperature of the upper subchannel at outlet (K)
T_{in}	inlet air temperature (K)

T_p	temperature of absorbing plate (K)
$T_{p,m}$	mean temperature of absorbing plate (K)
T_s	ambient temperature (K)
U_B	loss coefficient from the bottom of solar air heater to the ambient environment (W/(m ² K))
U_E	loss coefficient from the edge of solar air heater to the ambient environment (W/(m ² K))
U_L	overall loss coefficient (W/(m ² K))
U_T	loss coefficient from the top of solar air heater to the ambient environment (W/(m ² K))
V	wind velocity (m/s)
W	channel width (m)
Y_i	coefficient defined in Equations (A16) and (A17)

Greek Letters

α_p	absorptivity of the absorbing plate
η_i	collector efficiency for the flat-plate a and wire mesh packed
$\eta_{exp,i}$	experimental data of collector efficiency
$\eta_{theo,i}$	theoretical prediction of collector efficiency
η_w	collector efficiency of wire mesh solar air heater
τ_g	transmittance of glass cover
ε_g	emissivity of glass cover
ε_R	emissivity of bottom plate
ε_p	emissivity of absorbing plate
ρ	air density (kg/m ³)
μ	air viscosity (kg/(s m))
σ	Stefan-Boltzmann constant ($= 5.682 \times 10^{-8}$) (W/(m ² K ⁴))
ξ	dimensionless channel length

Appendix

The definitions of B_i , G_i , M_i , Y_i , k_i , F_i , and I_i :

$$B_1 = (h_{r1}h_b G_1 G_4 + h_b G_1 + U_{c1-s} h_b G_4)/M_b \quad (A1)$$

$$B_2 = (h_b G_2 + h_{r1}h_b G_2 G_4)/M_b \quad (A2)$$

$$B_3 = (h_b G_3 + h_{r1}h_b G_3 G_4)/M_b \quad (A3)$$

$$B_4 = (h_{r2}h_a G_5 G_7 + h_a G_5 - U_{B-s} h_a G_7)/M_a \quad (A4)$$

$$B_5 = (h_a G_6 + h_{r2}h_a G_6 G_7)/M_a \quad (A5)$$

$$B_6 = (h_a G_3 + h_{r2}h_a G_3 G_7)/M_a \quad (A6)$$

$$M_b = \left[\frac{-\dot{m}(1+R)C_p}{WL} \right] = -\dot{m}(1+R)C_p/A_c \quad (\text{A7})$$

$$M_a = \left[\frac{\dot{m}(1+R)C_p}{WL} \right] = \dot{m}(1+R)C_p/A_c \quad (\text{A8})$$

$$G_1 = -(h_a + U_T + U_B)/(h_a + h_b + U_T + U_B) \quad (\text{A9})$$

$$G_2 = h_a/(h_a + h_b + U_T + U_B) \quad (\text{A10})$$

$$G_3 = I_0 \alpha_p \tau_g^2 / (h_a + h_b + U_T + U_B) \quad (\text{A11})$$

$$G_4 = (h_b + h_{r,p-c1} + U_{c1-s})^{-1} \quad (\text{A12})$$

$$G_5 = -(h_b + U_T + U_B)/(h_a + h_b + U_T + U_B) \quad (\text{A13})$$

$$G_6 = h_b/(h_a + h_b + U_T + U_B) \quad (\text{A14})$$

$$G_7 = (h_a + h_{r,p-R} + U_{B-s})^{-1} \quad (\text{A15})$$

$$Y_1 = \frac{(B_1 + B_5) + \sqrt{(B_1 - B_5)^2 + 4B_2B_4}}{2} \quad (\text{A16})$$

$$Y_2 = \frac{(B_1 + B_5) - \sqrt{(B_1 - B_5)^2 + 4B_2B_4}}{2} \quad (\text{A17})$$

$$k_1 = \frac{B_4 \left[(I_2R - B_4)(F_2 + F_3) - I_2F_2e^{Y_2} - I_2Re^{Y_2}(F_2 + F_3) \right]}{F_1 \left[I_1I_2R(e^{Y_1} - e^{Y_2}) + B_4(I_1e^{Y_1} - I_2e^{Y_2}) \right]} \quad (\text{A18})$$

$$k_2 = \frac{-B_4 \left[(I_1R - B_4)(F_2 + F_3) - I_1F_2e^{Y_1} - I_1Re^{Y_1}(F_2 + F_3) \right]}{F_1 \left[I_1I_2R(e^{Y_1} - e^{Y_2}) + B_4(I_1e^{Y_1} - I_2e^{Y_2}) \right]} \quad (\text{A19})$$

$$F_1 = B_1B_5 - B_2B_4 \quad (\text{A20})$$

$$F_2 = B_3B_4 - B_1B_6 \quad (\text{A21})$$

$$F_3 = B_3B_5 - B_2B_6 \quad (\text{A22})$$

$$I_1 = Y_1 - B_4 - B_5 \quad (\text{A23})$$

$$I_2 = Y_2 - B_4 - B_5 \quad (\text{A24})$$

Conflicts of Interest

The authors declare no conflict of interest.

References

1. Chen, X.; Yang, H.; Lu, L.; Wang, J.; Liu, W. Experimental studies on a ground coupled heat pump with solar thermal collectors for space heating. *Energy* **2011**, *36*, 5292–5300.
2. Sharma, V.K.; Colangelo, A.; Spagna, G. Experimental performance of an indirect type solar fruit and vegetable dryer. *Energy Convers. Manag.* **1993**, *34*, 293–308.
3. Sreekumar, A. Techno-economic analysis of a roof-integrated solar air heating system for drying fruit and vegetables. *Energy Convers. Manag.* **2010**, *51*, 2230–2238.
4. Bari, E.; Noel, J.Y.; Comini, G.; Cortella, G. Air-cooled condensing systems for home and industrial appliances. *Appl. Therm. Eng.* **2005**, *25*, 1446–1458.
5. Chen, Z.; Gu, M.; Peng, D.; Peng, C.; Wu, Z. A Numerical study on heat transfer of high efficient solar flat-plate collectors with energy storage. *Int. J. Green Energy* **2010**, *7*, 326–336.
6. Seluck, M.K. *Solar Air Heaters and Their Applications*; Sayigh, A.A.M., Ed.; Academic Press: New York, NY, USA, 1977.
7. Kreith, F.; Kreider, J.F. *Principles of Solar Engineering*; McGraw-Hill: New York, NY, USA, 1978.
8. Tan, H.M.; Charters, W.W.S. Experimental investigation of forced-convective heat transfer for fully-developed turbulent flow in a rectangular duct with asymmetric heating. *Sol. Energy* **1970**, *13*, 121–125.
9. Yeh, H.M. Theory of baffled solar air heaters. *Energy* **1992**, *17*, 697–702.
10. Duffie, J.A.; Beckman, W.A. *Solar Engineering of Thermal Processes*, 3rd ed.; Wiley: New York, NY, USA, 2006.
11. Ramadan, M.R.I.; EL-Sebaei, A.A.; Aboul-Enein, S.; El-Bialy, E. Thermal performance of a packed bed double-pass solar air heater. *Energy* **2007**, *32*, 1524–1535.
12. Sopian, K.; Alghoul, M.A.; Alfegi, E.M.; Sulaiman, M.Y.; Musa, E.A. Evaluation of thermal efficiency of double-pass solar collector with porous—Nonporous media. *Renew. Energy* **2009**, *34*, 640–645.
13. Dhiman, N.K.; Tiwari, G.N. Performance of a two channel suspended flat plate solar air heater. *Energy Convers. Manag.* **1984**, *24*, 269–275.
14. Naphon, P. On the performance and entropy generation of the double-pass solar air heater with longitudinal fins. *Renew. Energy* **2005**, *30*, 1345–1357.
15. Ho, C.D.; Yeh, H.M.; Wang, R.C. Heat-transfer enhancement in double-pass flat-plate solar air heaters with recycle. *Energy* **2005**, *30*, 2796–2817.
16. Chiou, J.P.; El-Wakil, M.M.; Duffie, J.A. A slit-and-expanded aluminum-foil matrix solar collector. *Sol. Energy* **1965**, *9*, 73–80.
17. Choudhury, C.; Garg, H.P. Performance of air-heating collectors with packed airflow passage. *Sol. Energy* **1993**, *50*, 205–221.
18. Mittal, M.K.; Varshney, L. Optimal thermohydraulic performance of a wire mesh packed solar air heater. *Sol. Energy* **2006**, *80*, 1112–1120.
19. Öztürk, H.H.; Demirel, Y. Exergy-based performance analysis of packed-bed solar air heaters. *Int. J. Energy Res.* **2004**, *28*, 423–432.

20. Kolb, A.; Winter, E.R.F.; Viskanta, R. Experimental studies on a solar air collector with metal matrix absorber. *Sol. Energy* **1999**, *65*, 91–98.
21. El-Sebaei, A.A.; Aboul-Enein, S.; Ramadan, M.E.I.; Shalaby, S.M.; Moharram, B.M. Investigation of thermal performance of double-pass flat and v-corrugated plate solar air heaters. *Energy* **2011**, *36*, 1076–1086.
22. Marquart, R.; Blenke, H. Circulation of moderately to highly viscous Newtonian and non-Newtonian liquids in propeller-pumped circulating loop reactors. *Int. Chem. Eng.* **1980**, *20*, 368–378.
23. Dussap, G.; Gros, J.B. Energy consumption and interfacial mass transfer area in an air-lift fermentor. *Chem. Eng. J.* **1982**, *25*, 151–162.
24. Jones, A.G. Liquid circulation in a drift-tube bubble column. *Chem. Eng. Sci.* **1985**, *40*, 449–462.
25. Ho, C.D.; Yeh, H.M.; Guo, J.J. An analytical study on the enrichment of heavy water in the continuous thermal diffusion column with external refluxes. *Sep. Sci. Technol.* **2002**, *37*, 3129–3153.
26. Ho, C.D.; Lin, C.S.; Chuang, Y.C.; Chao, C.C. Performance improvement of wire mesh packed double-pass solar air heaters with external recycle. *Renew. Energy* **2013**, *57*, 479–489.
27. Varshney, L.; Saini, J.S. Heat transfer and flow friction factor correlations for rectangular solar air heater duct packed with wire mesh screen matrices. *Sol. Energy* **1998**, *62*, 255–262.
28. Chang, W.S. Porosity and effective thermal conductivity of wire screens. *J. Heat Transf.* **1990**, *112*, 5–9.
29. Kays, W.M. *Convective Heat and Mass Transfer*; McGraw-Hill: New York, NY, USA, 1996.
30. Heaton, H.S.; Reynolds, W.C.; Kays, W.M. Heat transfer in annular passages. Simultaneous development of velocity and temperature fields in laminar flow. *Int. J. Heat Mass Transf.* **1964**, *7*, 763–781.
31. Saini, R.P.; Saini, J.S. Heat transfer and friction factor correlation for artificially roughened ducts with expanded metal mesh as roughness element. *Int. J. Heat Mass Transf.* **1997**, *40*, 973–986.
32. Klein, S.A. Calculation of flat-plate loss coefficients. *Sol. Energy* **1975**, *17*, 79–80.
33. Hottel, H.C.; Woetz, B.B. The performance of flat-plate solar heat collectors. *Trans. ASME* **1942**, *64*, 91–104.
34. McAdams, W.H. *Heat Transmission*, 3rd ed.; McGraw-Hill: New York, NY, USA, 1954.
35. Prasad, S.B.; Saini, J.S.; Singh, K.M. Investigation of heat transfer and friction characteristics of packed bed solar air heater using wire mesh as packing material. *Sol. Energy* **2009**, *83*, 773–783.
36. Bird, R.B.; Stewart, W.E.; Lightfoot, E.N. *Transport Phenomena*; 2nd ed.; Wiley: New York, NY, USA, 2007.
37. Mohseni-Languri, E.; Taherian, H.; Masoodi, R.; Reisel, J.R. An energy and exergy study of a solar thermal air collector. *Therm. Sci.* **2009**, *13*, 205–216.
38. Mohseni-Languri, E.; Taherian, H.; Hooman, K.; Reisel, J.R. Enhanced double-pass solar air heater with and without porous medium. *Int. J. Green Energy* **2011**, *8*, 643–654.